water

MDPI

Article

Spatio-Temporal Analysis and Contribution of Agricultural Drought in Daling River Basin: A VIC Model-Based Soil Moisture Simulation and SMAPI Evaluation

Mei Ding [1,2], Juan Lv [1,*], Yanping Qu [1,*] and Tianliang Jiang [1]

[1] Research Center on Flood and Drought Disaster Reduction, China Institute of Water Resources and Hydropower Research, Beijing 100038, China; dingmei9553@163.com (M.D.); jiangtl@iwhr.com (T.J.)
[2] Miyun District Emergency Management Bureau of Beijing Municipality, Beijing 101599, China
* Correspondence: lujuan@iwhr.com (J.L.); quyp@iwhr.com (Y.Q.)

Abstract: Soil moisture is a crucial factor that directly influences agricultural drought. As such, investigating drought-monitoring methods utilizing soil moisture data is of significant importance for accurately evaluating and predicting agricultural drought. However, the current soil moisture data for the Daling River Basin is insufficient. Therefore, the variable infiltration capacity (VIC) hydrological model was utilized to simulate soil moisture in the Daling River Basin. The simulated data were then analyzed in conjunction with the standardized moisture anomaly index (*SMAPI*) to analyze and evaluate the spatio-temporal characteristics of agricultural drought in the Darling River Basin. The results indicate that the frequency of drought occurrence in the basin follows a seasonal pattern of winter > spring > autumn > summer. Between 1981 and 2019, 24 out of 39 years experienced slight or greater drought, 15 years experienced moderate or more severe drought, and 4 years experienced severe drought. Drought conditions have become exceptionally severe in the 21st century. Specifically, the frequency of drought occurrence from 2001 to 2019 was nearly 10 times higher compared to the period from 1981 to 2000. The droughts were most severe in the southeast and southwest of the Daling River Basin, while the northeast and northwest experienced relatively mild drought. Agricultural drought is influenced by numerous complex factors. The contribution of climate change (*CC*) and other factors (*OF*) to agricultural drought was quantified by using a partial derivative under six different scenarios. Results showed that *SMAPI* was positively correlated with precipitation and solar radiation, while negatively correlated with temperature. From 1981 to 2000, *SMAPI* exhibited an increasing trend that accounted for 61.66% of variability, while a decreasing trend accounted for 38.34%. From 2001 to 2019, *SMAPI* exhibited a significant decreasing trend that accounted for 93.53% of the variability, while the increasing trend only accounted for 6.47%. *CC* was the dominant factor in most of the areas with increased *SMAPI*. *OF* was the main controlling factor for areas with decreased *SMAPI*.

Keywords: VIC model; soil moisture; agricultural drought; Daling River Basin

check for updates

Citation: Ding, M.; Lv, J.; Qu, Y.; Jiang, T. Spatio-Temporal Analysis and Contribution of Agricultural Drought in Daling River Basin: A VIC Model-Based Soil Moisture Simulation and SMAPI Evaluation. *Water* **2023**, *15*, 3809. https://doi.org/10.3390/w15213809

Academic Editor: Luís Filipe Sanches Fernandes

Received: 15 September 2023
Revised: 24 October 2023
Accepted: 25 October 2023
Published: 31 October 2023

1. Introduction

Soil moisture is a crucial factor in agricultural drought monitoring as it directly impacts the water and energy exchange between the surface and the atmosphere interface [1,2]. In agricultural applications, soil moisture is a more direct influencing factor than precipitation [3]. Agriculture is most directly and severely affected by drought, and changes in soil moisture reflect many climatic variables, vegetation, and soil characteristics as a comprehensive index [4–6]. Thus, soil moisture is a key factor in the occurrence and development of drought. The value of soil moisture is essential in determining whether agricultural drought occurs, which directly determines the degree of agricultural drought [7–11].

Obtaining soil moisture data on a large scale is challenging and primarily depends on three methods: site monitoring; remote sensing; and hydrological simulation. Soil moisture station monitoring has some limitations, including a small number of stations nationwide, a short monitoring time series, and uneven spatial distribution of stations [12]. Although remote-sensing technology compensates for the limited coverage of the monitoring stations, it can only monitor the moisture of the soil surface up to 0–20 cm and cannot reflect the soil root water that affects the growth and development of crops [7]. In contrast, distributed hydrological models based on physical mechanisms can comprehensively consider precipitation, vegetation, soil characteristics, and other factors. These models can overcome the limitations of soil moisture stations and remote-sensing monitoring, providing soil moisture data with a long time series, uniform spatial distribution, and at different depths.

The VIC Model is widely used as it is a large-scale distributed hydrological model with good simulation ability [13,14]. Studies have shown that using the daily soil moisture simulated by the VIC model to build a daily-scale drought index can accurately reflect the actual drought conditions [15]. Ye Zhu applied the VIC model to construct a new Palmer index that can achieve short-term drought monitoring [16]. Other studies by Fan et al. [17], Leng et al. [18], Wu et al. [19] and others have demonstrated the efficacy of using the VIC model to simulate soil moisture for describing and expressing agricultural drought. The simulation values can replace measured values for drought research. The impact of drought disasters is far-reaching, and it is necessary to study the dynamic monitoring of agricultural drought [20,21]. The mechanism of drought disasters is complex, and a comprehensive understanding of the spatio-temporal distribution characteristics of agricultural drought and quantitative analysis of the response relationship between climate factors and other factors to drought is a prerequisite for conducting research on drought disaster risk [22].

This study selected the Daling River Basin as the study area. The daily soil moisture of the watershed was simulated by the VIC model, and the spatio-temporal variation characteristics of drought were analyzed from aspects such as drought coverage area, drought frequency, and drought intensity using *SMAPI*. The response of *SMAPI* to major meteorological factors was identified using partial correlation coefficients and multiple linear regression equations. The objective was to reveal the regional characteristics and influencing factors of drought disasters in the Daling River Basin and provide a basis for drought-risk monitoring and assessment in the region.

2. Materials and Methods

2.1. Study Area

Daling River Basin, located in northwest Liaoning Province, China, is the largest river in the region (Figure 1). It is prone to frequent agricultural drought, and the widespread cultivation of crops exacerbates the drought risk, leading to the saying “nine droughts in ten years”. Its geographical location, climate type, hydrometeorology, and soil type are shown in Table 1. The upper reaches of the Daling River Basin are joined by two rivers in the north and south directions and are injected into the Bohai Sea through Linghai station. In this study, Linghai hydrological station is selected to control the basin, and there are five weather stations in total.

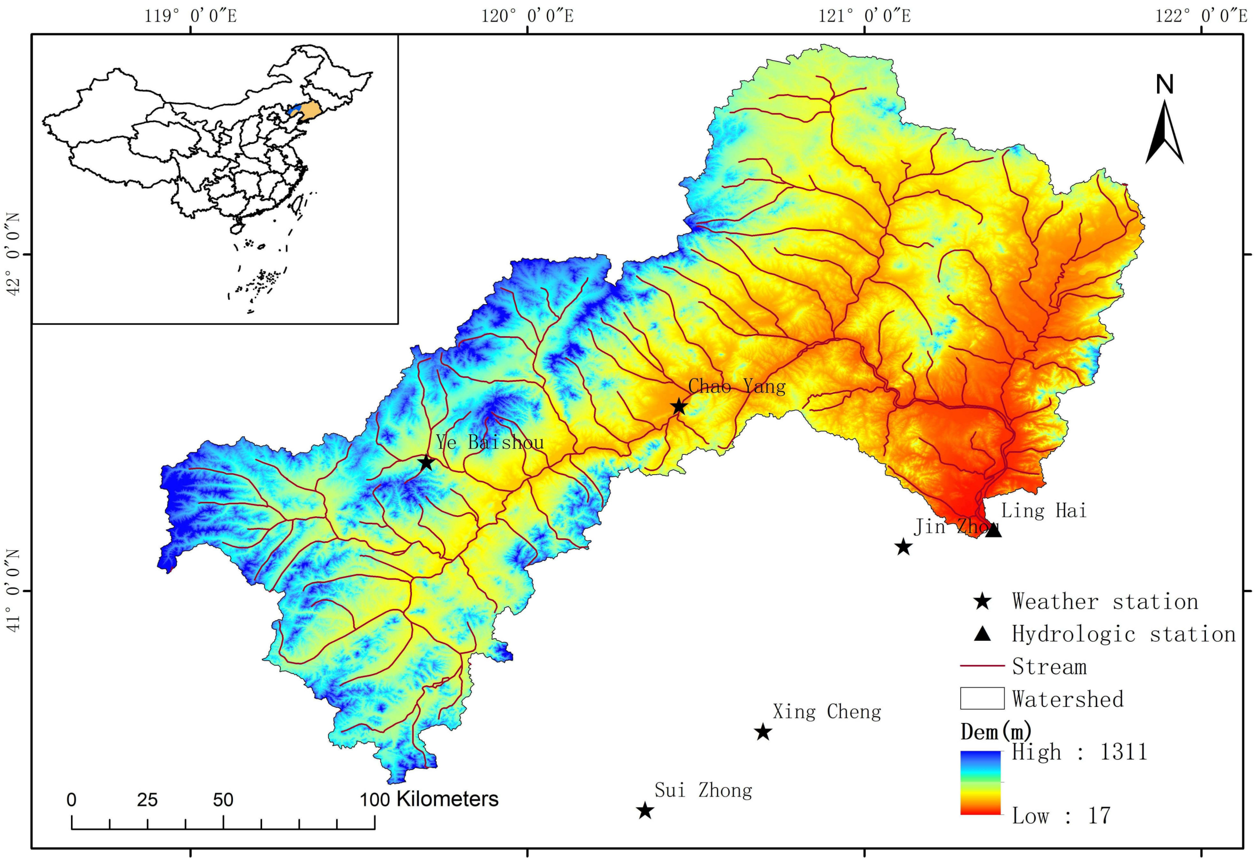

Figure 1. Location of the study area.

Table 1. Overview of Daling River Basin [23–25].

Study Area	Geographic Location	Drainage Area	Climate Type	Hydrometeorological Characteristics	Topographical Conditions	Soil Type	Drought Situation
Control basin of Linghai hydrological station of Daling River	Northwest Liaoning Province, 119°00′–122°00′ E, 40°30′–42°30′ N	23,057 km^2	Temperate continental monsoon climate, cold and dry in winter, hot and humid in summer, dry and windy in spring and autumn.	The average precipitation is 400~600 mm, the average temperature is 7~10 °C, the average wind speed is 2~3 m/s, the average evaporation is 900~1200 mm, and the average runoff is 1.633 billion m^3.	Low mountain and hilly area, 17~1311 M above sea level, and the terrain decreases from west to east.	Mainly brown soil, combined with brown forest soil.	There were 10 major droughts from 1901 to 1949. In the 20 years from 1959 to 1978, there were 10 Spring Droughts and 8 autumn droughts. In 2009, it suffered the most serious historical drought in 60 years, and in 2015, Liaoning suffered the most serious drought in 64 years. A major drought occurs on average every 6–7 years.

2.2. Data Sources and Preprocessing

The data used in the study include meteorological data, DEM digital elevation data, vegetation data, soil data, and hydrological data used for VIC Model simulation. Drought data are used for drought-monitoring verification. See Table 2 for data types and sources.

Table 2. Data used in the study.

Data Type	Data Name	Data Source
Meteorological data	Daily precipitation, daily average temperature and daily average wind speed from 1981 to 2019	China Meteorological Data Network (http://data.cma.cn/url: accessed on 20 October 2022)
Hydrological data	Daily runoff from 1981 to 2017	National water and rain information website (http://xxfb.mwr.cnurl: accessed on 20 October 2022)
DEM	SRTM 90 m resolution digital elevation	Geospatial data cloud (http://www.gscloud.cn/searchurl: accessed on 20 May 2018)
Vegetation data	China WESTDC series land cover data products	Science and technology center in cold and dry regions (http://www.landcover.org/data/landcover/data.shtmlurl: accessed on 20 May 2022)
Soil data	5 min FAO soil map of the world	Food and Agriculture Organization of the United Nations (http://www.fao.org/statistics/zh/url: accessed on 20 May 2022)
Drought data	Drought-affected area of crops from 2004 to 2014	Statistical system for flood control and Drought Relief (Dynamic Statistics of Agricultural Drought)

Among them, the meteorological data were used as the forcing data of the model, and the 90 m DEM data were used for the grid division of the model. In order to match the simulation grid with the DEM, the research area was divided into a 9 km × 9 km spatial resolution grid and ran through the VIC Model. Vegetation data and soil data were used as input data of the model. Runoff data from Linghai hydrological station in Daling River Basin were used for model calibration and validation.

According to the crop drought area data in the agricultural drought dynamic statistical table of the flood control and drought relief statistical system, the total drought area of crops in Liaoning Province from 2004 to 2014 was calculated on an annual scale (Table 3).

Table 3. Statistical table of crop drought-affected areas in Liaoning from 2004 to 2014 (10^3 hm^2).

Year	2004	2005	2006	2007	2008	2009	2010	2011	2012	2013	2014
Liaoning	240.32	1.47	5350.29	6567.58	785.18	31,366	2065.82	951.76	122.19	1312.44	23.34

2.3. Methodology

The Daling River Basin was divided into 433 grids by Arc GIS, and grid data of daily precipitation, temperature, and wind speed from 1981 to 2019 were obtained through the spatial interpolation method as meteorological forcing data for the VIC model. The inverse-distance weighted interpolation method, considering elevation, was used for spatial interpolation of precipitation and temperature, as they exhibited a good gradient relationship with elevation. Only the inverse-distance weighted interpolation method was used for wind speed interpolation, as it has a small impact on the accuracy of model simulation. The soil and vegetation data were generated from the global 1 km land vegetation cover data and the global 10 km soil database as corresponding parameter files, which together serve as input files to run the VIC model. The runoff data from hydrological stations were used to calibrate and validate the accuracy of the simulation. The simulated soil moisture data were combined with *SMAPI* to monitor the drought in the watershed, and the drought-affected area of crops was used to verify the monitoring results. Second-order partial correlation analyses were used to study the correlation between climate factors and *SMAPI*, and the multiple linear regression approach was used to quantify the impact of climate factors and other factors on *SMAPI* in the Daling River Basin. Quantitative analysis was conducted on the contributions of climate change (*CC*) and other factors (*OF*), such as human activities, to agricultural drought. See Figure 2 for details.

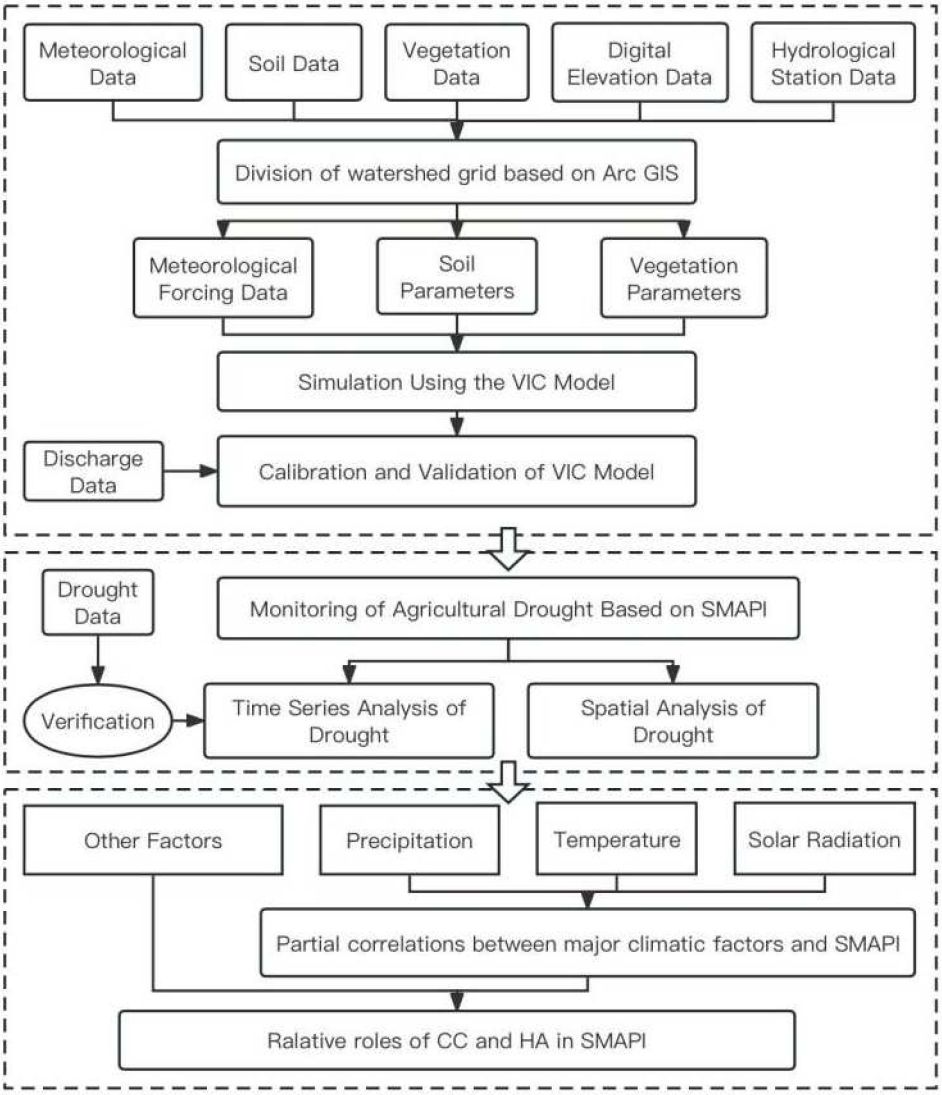

Figure 2. Flow chart of this study.

2.3.1. Soil Moisture Simulation

The study used the VIC model to simulate the soil moisture of the basin, which is also known as the "variable infiltration capacity model". The VIC model is a grid based semi-distributed, large-scale hydrological model that considers the effects of vegetation, terrain, and soil on the exchange of moisture and energy between land and atmosphere [26–28]. The model takes into account the influence of spatial heterogeneity of precipitation and soil heterogeneity within the sub grid, which makes up the deficiency of traditional hydrological models in describing energy processes [29]. One of its major outputs is runoff, which is a direct and important part of the water cycle that the model seeks to simulate. While soil moisture is a crucial parameter, it is not the only factor determining runoff production. Other variables such as precipitation, evapotranspiration, and the physical characteristics of the watershed also play significant roles. Therefore, using runoff data for validation can better capture the integrated effect of these factors, providing a more comprehensive evaluation of the model's performance. The research shows that the VIC model has a good ability to simulate a wide range of soil moisture [30,31]. Using runoff data for both calibration and validation can help to ensure consistency and reliability in the model's performance evaluation [32–34].

In this study, calibrations were made manually and the simulation results are calibrated and validated with the observed monthly runoff values. The multi-year relative error (Equation (1)) and the Nash–Sutcliffe model efficiency coefficient (Equation (2)) were used as the objective functions, which describe the degree of process line matching between simulated and observed values [35].

$$E_r = (\overline{Q}_c - \overline{Q}_0)/\overline{Q}_0 \tag{1}$$

where $\overline{Q}_0$ and $\overline{Q}_c$ are the mean observed and simulated runoffs, respectively.

The relative error reflects the total amount of accuracy. The smaller the absolute value, the higher the simulation precision.

$$C_e = \frac{\sum(Q_{i,0} - \overline{Q}_0)^2 - \sum(Q_{i,c} - Q_{i,0})^2}{\sum(Q_{i,0} - \overline{Q}_0)^2} \tag{2}$$

where $Q_{i,0}$ and $Q_{i,c}$ are the observed and simulated runoffs, respectively.

The Nash efficiency coefficient reflects the flow process of runoff. The larger the value, the better the process fitting and the higher the simulation accuracy.

2.3.2. Agricultural Drought Assessment

SMAPI (soil moisture anomaly percentage index) is the most basic and widely used index based on soil moisture, which takes into account the dynamic change characteristics of soil moisture in different regions. *SMAPI* is a dimensionless relative drought index, which can be used to compare drought characteristics of different regions in different periods. It is defined as the degree to which the simulated soil moisture deviates from the multi-year average [35]. The calculation is shown in Equation (3).

$$SMAPI = \frac{m - \overline{m}}{\overline{m}} \times 100\% \tag{3}$$

where m is the current soil moisture; $\overline{m}$ is the average soil moisture in the same period, which can also be regarded as the climatic suitable value of soil moisture.

The division standard of drought level based on the *SMAPI* was determined using the comprehensive frequency distribution method proposed by Wu et al. [9]. The frequency distribution of *SMAPI* has small regional differences and can be integrated into a curve, which can be used to compare the degree of drought in different regions. The daily *SMAPI* values of the Daling River Basin from 1981 to 2019 were calculated in descending order. The occurrence probability of 0.005 was defined as extreme drought, and the probability of 0.02 was defined as severe drought. The specific probability and classification criteria for drought levels are shown in Table 4.

Table 4. Assessment criteria for drought level of *SMAPI*.

Drought Level	Frequency	*SMAPI*/%
Extreme drought	0.005	≤ -18
Severe drought	0.020	$-18 \sim -14$
Moderate drought	0.100	$-14 \sim -9$
Slight drought	0.200	$-9 \sim -3.85$
Non-drought	0.675	≥ -3.85

2.3.3. Partial Correlation

Second-order partial correlation analyses were used to eliminate the interference of other variables and analyze the correlation between climate factors and *SMAPI* [36–38].

The partial correlation coefficients of the grid-scale between *SMAPI* and temperature, precipitation, and solar radiation were calculated according to Equation (4).

$$r_{xy,z\lambda} = \frac{r_{xy,z} - r_{x\lambda,z} \times r_{y\lambda,z}}{\sqrt{1 - r_{x\lambda,z}^2} \times \sqrt{1 - r_{y\lambda,z}^2}} \quad (4)$$

where x and y are the factors used to calculate the partial correlation coefficient, and z and λ are the control variables. $r_{xy,z\lambda} > 0$ indicates a positive correlation between variables x and y; $r_{xy,z\lambda} < 0$ indicates a negative correlation between variables x and y.

The t-test is usually used as a significance test method for the partial correlation coefficient, and the calculation is shown in Equation (5).

$$t = \frac{r_{xy,z\lambda}}{\sqrt{1 - r_{xy,z\lambda}^2}} \sqrt{n - m + 1} \quad (5)$$

where t is the significance test coefficient, n is the number of samples, m is the number of independent variables, and the critical values for different significance levels can be obtained by looking up the t-distribution table.

2.3.4. Quantifying the Contributions to *SMAPI*

In order to quantify the response of climate change and other factors to *SMAPI*, precipitation, temperature, and solar radiation were selected as key climate factors in this study. However, the response of climate factors to *SMAPI* may not be entirely linear, and the selection of a nonlinear model requires a detailed statistical analysis of various types of data. In addition, similar studies have shown that multiple linear regression models can also perform well [39,40]. Considering that the purpose of the study is to reveal an empirical regulation—the extent to which climate change and other factors affect *SMAPI*—we established a multiple linear regression method among the annual *SMAPI*, precipitation, temperature, and solar radiation. The calculation is shown in Equation (6).

$$y = a \times P + b \times T + c \times SR + \varepsilon \quad (6)$$

where y is the annual *SMAPI*, P, T, and SR are the annual average temperature, annual precipitation, and annual average solar radiation, respectively, a, b, and c are the fitted regression coefficients, and ε is the residual error term.

CC represents climate change; *OF* represents other factors. The partial derivative method was used to evaluate the contributions of *CC* and *OF* to *SMAPI*, and the calculation formula is shown in Equation (7).

$$K = CC_{con} + OF_{con} = P_{con} + T_{con} + SR_{con} + OF_{con} \approx \frac{\partial y}{\partial P} \times \frac{dP}{dt} + \frac{\partial y}{\partial T} \times \frac{dT}{dt} + \frac{\partial y}{\partial SR} \times \frac{dSR}{dt} + OF_{con} \quad (7)$$

where K is the *SMAPI* trend and CC_{con} is the contribution of *CC*, which includes P_{con} (contribution of precipitation), T_{con} (contribution of temperature), and SR_{con} (contribution of solar radiation); OF_{con} is the contribution of *OF*, equal to the residual between K and CC_{con}. t is the research period. $\frac{\partial y}{\partial P}$ and $\frac{dP}{dt}$ are the slope of the linear regression equation between *SMAPI* and precipitation, and the slope of the linear regression equation between precipitation and year, respectively. A similar definition is suitable for $\frac{\partial y}{\partial T}$, $\frac{\partial y}{\partial SR}$, $\frac{dT}{dt}$, and $\frac{dSR}{dt}$.

According to the driving mechanism, the contribution of driving factors can be divided into six scenarios, as shown in Table 5 [38].

Table 5. Contribution calculations and corresponding scenarios of the driving factors of *SMAPI*.

	K	**Driving Factors**	CC_{con}	OF_{con}	**Contribution (%)**		**Scenario**
					CC	**OF**	
Increasing *SMAPI*	>0	*CC* and *OF*	>0	>0	$\frac{\lvert CC_{con}\rvert}{\lvert CC_{con}\rvert+\lvert OF_{con}\rvert}$	$\frac{\lvert OF_{con}\rvert}{\lvert CC_{con}\rvert+\lvert OF_{con}\rvert}$	ICO
		CC	>0	<0	100	0	IC
		OF	<0	>0	0	100	IO
Decreasing *SMAPI*	<0	*CC* and *OF*	<0	<0	$\frac{\lvert CC_{con}\rvert}{\lvert CC_{con}\rvert+\lvert OF_{con}\rvert}$	$\frac{\lvert OF_{con}\rvert}{\lvert CC_{con}\rvert+\lvert OF_{con}\rvert}$	DCO
		CC	<0	>0	100	0	DC
		OF	>0	<0	0	100	DO

Abbreviations: *SMAPI*, soil moisture anomaly percentage index; *K*, slope of *SMAPI*; *CC*, climate change; *OF*, other factors; ICO, *SMAPI* increase due to *CC* and *OF*; IC, *SMAPI* increase due to *CC*; IO, *SMAPI* increase due to *OF*; DCO, *SMAPI* decrease due to CC and *OF*; DC, *SMAPI* decrease due to *CC*; DO, *SMAPI* decrease due to *OF*.

The slope calculation formula is shown in Equation (8).

$$K = \frac{n \times \sum_{i=1}^{n} i \times SMAPI_i - \sum_{i=1}^{n} i \sum_{i=1}^{n} SMAPI_i}{n \times \sum_{i=1}^{n} i^2 - \left(\sum_{i=1}^{n} i\right)^2} \tag{8}$$

where K represents the slope of linear regression, i represents the year of the independent variable, n is 39 years, and $SMAPI_i$ is the *SMAPI* value in the i year; $K > 0$ indicates an increase in *SMAPI* over time, while $K < 0$ indicates a decrease in *SMAPI* over time.

3. Results

In this paper, the VIC model was used to simulate the soil moisture of Daling River Basin and *SMAPI* was used to describe the spatio-temporal distribution characteristics of agricultural drought in the basin. A partial correlation coefficient statistical method was used to analyze the impact of climate factors on agricultural drought, and then to analyze the contribution of climate factors and other factors to agricultural drought.

3.1. VIC Model Simulation

The daily observed discharge data over the period 1981–1999 was chosen for model warm-up, the period of 2000–2010 was chosen for model calibration and parameter optimization, and the period of 2011–2017 was chosen for validation. The VIC model has six main parameters to calibrate [41,42], and it has no automated optimization function, which makes the parameter optimization difficult. Eventually, the best daily simulation results were obtained by manual adjustment of parameters. In this study, the multi-year relative error and the Nash–Sutcliffe model efficiency coefficient were used as the objective functions [43], which describe the total accuracy and the matching extent of the hydrograph between the simulated and observed values. During the calibration period, the relative error of the Daling River Basin was 0.07 and the Nash efficiency coefficient was 0.58. The relative error of the Daling River Basin was −0.09 and the Nash efficiency coefficient was 0.67 during the validation period.

Figure 3 gives the observed and simulated monthly discharge processes in the Daling River Basin. The simulated results show a hydrograph trend that is largely consistent with the observed discharge. However, due to the uncertainty and limitations of the VIC model, there were general errors in model simulation. On the one hand, the VIC model had a complex structure and a large parameter system. Although the determination of parameters was given a clear physical meaning, generalization, homogenization, and formula, calculation methods were still used to determine the parameters, resulting in uncertainty in the model. On the other hand, the VIC model simulated natural runoff without considering the impact of human activities, and the measured data obtained in this study had human interference factors that affected the simulation results. Overall, the results demonstrate the VIC model's effectiveness for simulating soil moisture in the Daling River Basin.

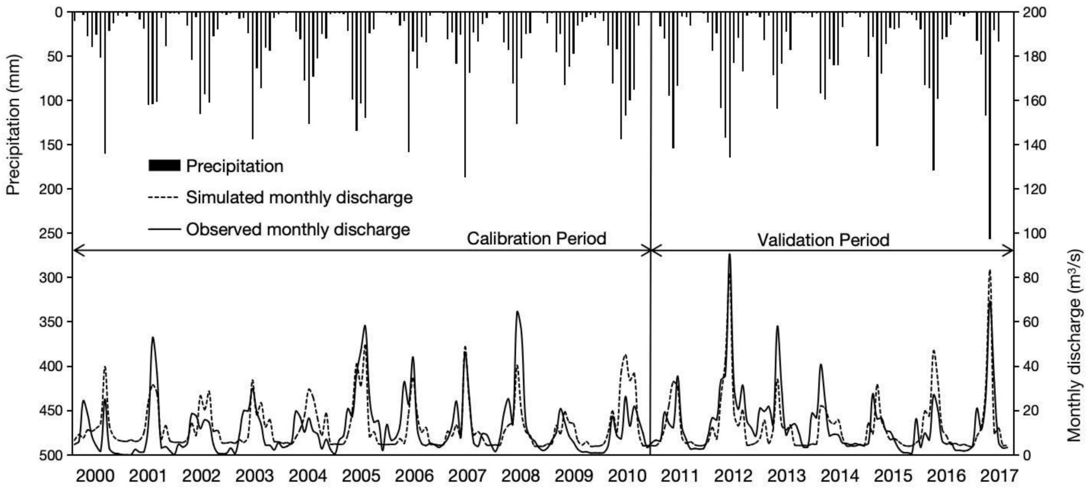

Figure 3. Observed and simulated monthly discharge during the calibration and validation period.

3.2. Monitoring and Evaluation of Agricultural Drought

3.2.1. Time Series Analysis of Drought

1. Analysis of annual drought characteristics

In order to analyze the interannual drought of the basin, the *SMAPI* values and the precipitation distribution of the corresponding time series were counted to analyze the annual-scale drought characteristics. According to Figure 4, the Daling River Basin was relatively wet from 1994 to 1999, and relatively dry after the 21st century. In 39 years, there were 24 years of slight-or-above drought, 15 years of moderate-or-above drought, and 4 years of severe drought, respectively, in 2009, 2010, 2012, and 2018. In particular, moderate and severe drought occurred for 8 consecutive months from August 2009 to March 2010, Slight, moderate, and severe drought occurred for 6 consecutive months from October 2011 to March 2012, and moderate and severe drought occurred for 7 consecutive months from July 2015 to February 2016.

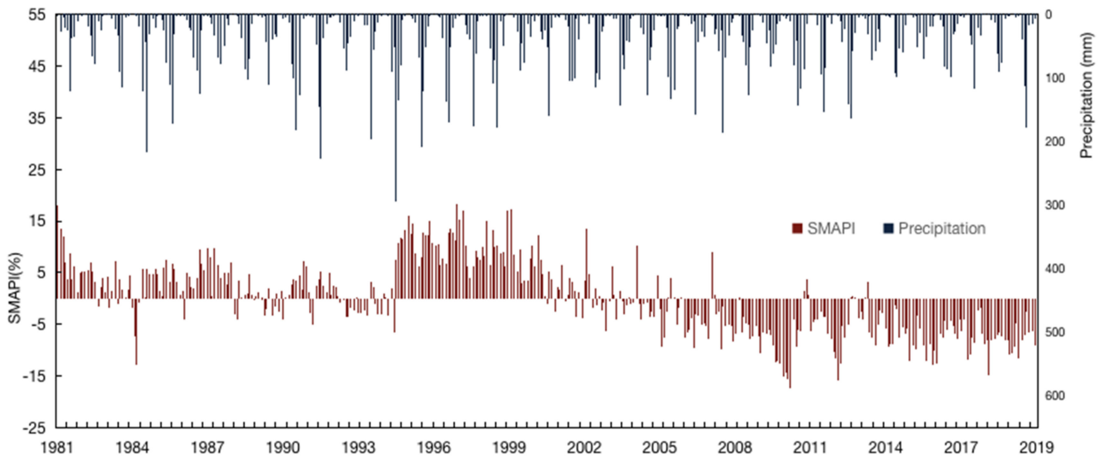

Figure 4. Time series change in *SMAPI* and precipitation in Daling River Basin.

According to the statistical data of the drought-affected area of crops in Liaoning Province on an annual scale from 2004 to 2014, the most serious year of agricultural drought in Liaoning Province was 2009, and the agricultural drought was also serious in 2006, 2007, and 2010. The statistical results of the drought-affected area of crops are consistent with the results of this study, indicating that the method used in this study is reasonable and feasible.

The scatter line in Figure 5 shows the annual actual change trend, while the dashed short line shows the decadal change trend. The average drought coverage rate of Daling River Basin was 35% from 1981 to 2019, and the drought coverage rate was more than 80% for 10 years. The largest drought coverage area was 98% in 2009, and the drought coverage rate was 0 from 1994 to 1999, with a large interannual difference. The average drought coverage area from 1981 to 2000 was 6.84%, but from 2001 to 2019, the average drought coverage area reached 64.65%, with an increase of nearly 10 times, indicating a clear trend of drought. As shown in the figure, a sudden drought occurred in 2006. In the middle of summer, there was a continuous period of sunny, hot, and rainy weather. In 2006, the western region of Liaoning Province was evaluated as the most severe drought since the founding of the People's Republic of China [44].

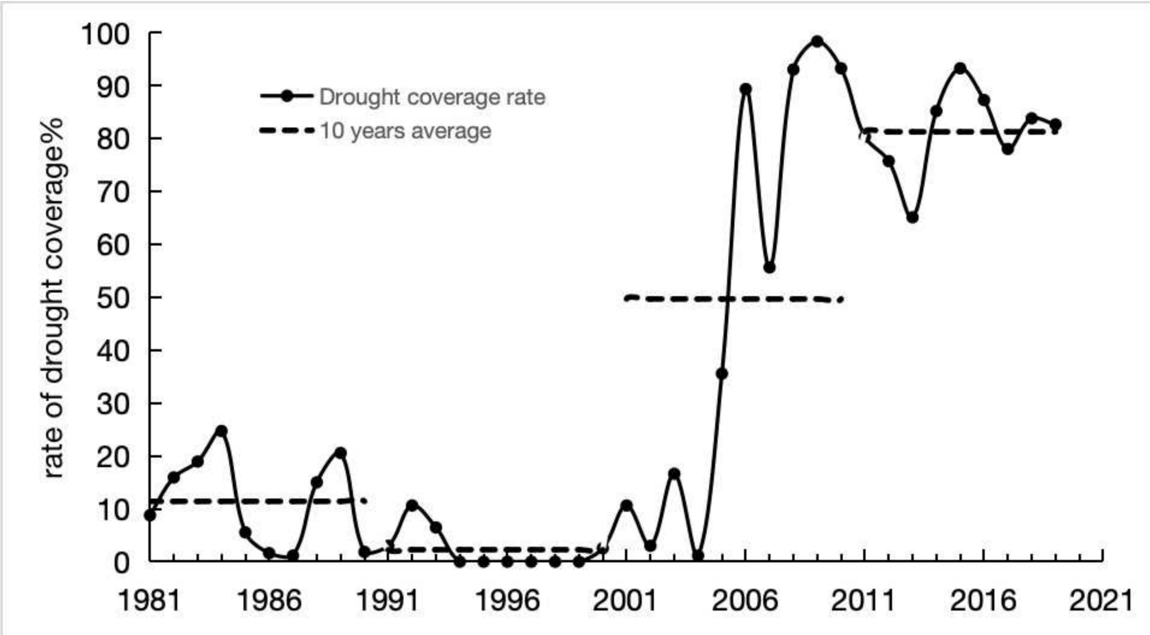

Figure 5. Annual drought coverage rate of Daling River Basin.

2. Analysis of seasonal drought characteristics

The *SMAPI* values of the Daling River Basin from 1981 to 2019 were calculated. According to the data in Table 4, the frequencies of drought in the basin in the four seasons were calculated as shown in Table 6.

Table 6. Seasonal drought frequency distribution in Daling River Basin.

Drought Grade	Extreme Drought	Severe Drought	Moderate Drought	Slight Drought	Non-Drought
Spring	0.008	0.014	0.074	0.226	0.678
Summer	0	0.011	0.078	0.202	0.709
Autumn	0.006	0.011	0.099	0.177	0.707
Winter	0.007	0.047	0.123	0.195	0.629

According to Table 6, the frequency of drought occurrence in the Daling River Basin is winter > spring > autumn > summer. Severe drought occurs most frequently in winter, followed by spring, autumn, and summer; the frequency of moderate drought occurrence is winter > autumn > summer > spring; the probability of slight drought occurring in spring is the highest, followed by summer, winter, and autumn. Daling River Basin is dry in winter and spring, hot in summer, and dry and windy in spring and autumn. There is less rainfall from winter to early summer, resulting in a tendency towards drought in winter and spring, which is basically consistent with previous studies [45–47]. Based on the information provided, it seems that the Daling River Basin is more influenced by precipitation regulation and storage.

By analyzing the drought coverage area of the Daling River Basin in the four seasons from 1981 to 2019 (Figure 6), it can be seen that the average drought coverage areas in the four seasons of spring, summer, autumn, and winter are 34.6%, 32.96%, 32.64%, and 38.85, respectively. Among them, there were 8 years when spring drought coverage exceeded 80%, with 2010 having the largest coverage at 98.6%, along with 5 years having 0% coverage (Figure 6a). For summer, 9 years had over 80% coverage, with 2009 having the maximum at 98.4%, and 8 years had 0% (Figure 6b). In autumn, coverage surpassed 80% in 10 years, with 2009 and 2015 exceeding 98%, and 7 years having 0% (Figure 6c). Finally, winter had over 80% coverage in 12 years, with 2009 and 2010 over 98%, and 6 years being 0% (Figure 6d).

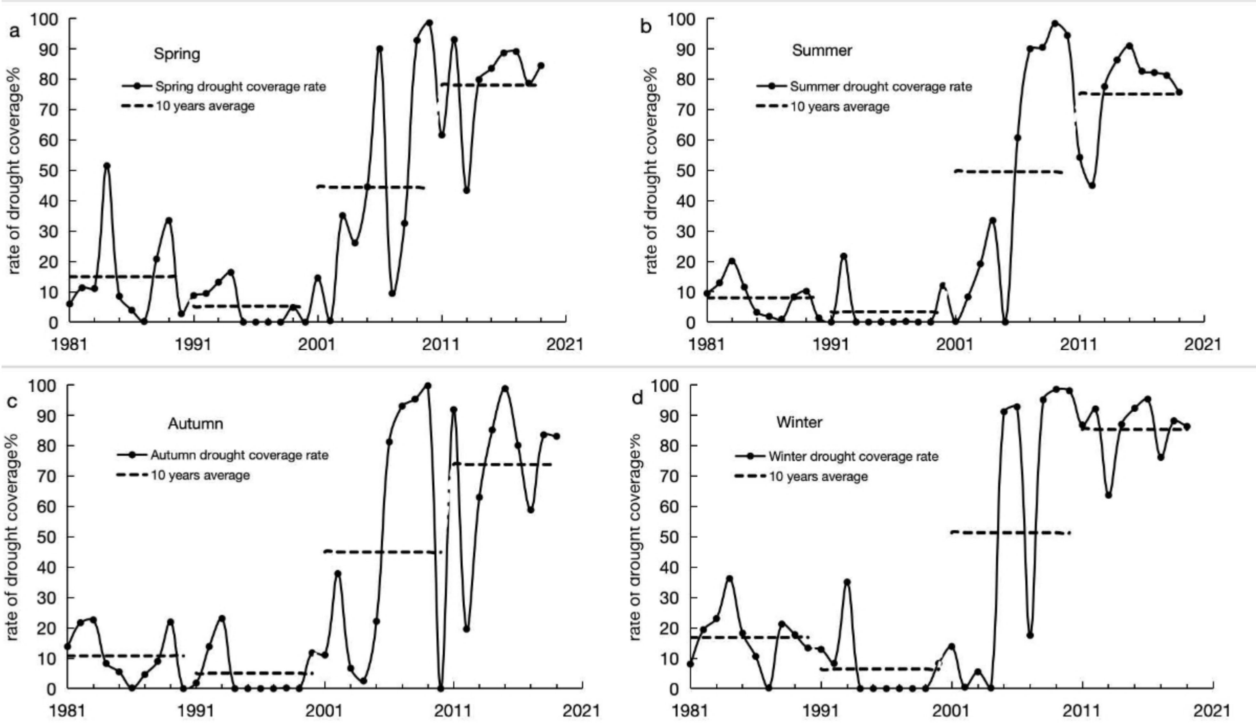

Figure 6. Seasonal drought coverage rate of Daling River Basin.

3.2.2. Analysis of Spatial Characteristics of Drought

3. Distribution characteristics of drought frequency

The annual drought frequency of Daling River Basin is between 26–44%, showing a regional distribution pattern of high frequency in the north and low frequency in the south (Figure 7). The frequency of drought in the northern, western, and central regions is relatively high, reaching over 36%, while the frequency of drought in the southeastern and southwestern regions is relatively low, both below 33%. The frequency of drought occurrence in most other regions ranges from 33% to 36%.

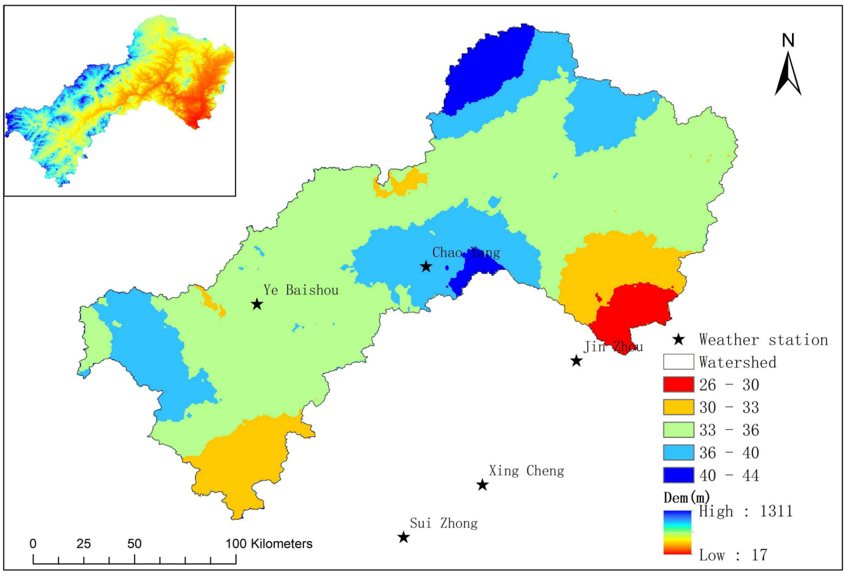

Figure 7. Annual drought frequency distribution of Daling River Basin.

Figure 8 shows the frequency of drought in the four seasons of Daling River Basin. The regional differences of drought frequency in the four seasons are small, ranging from 24% to 42%. In spring, the higher frequency occurs in the northeast to northwest of Daling River Basin, and the lower frequency occurs in the southeast and southwest (Figure 8a). In summer, only some areas in the northeast and northwest have a higher frequency of occurrence, while most other areas have a frequency below 35% (Figure 8b). In autumn, except for the northeast and northwest, the central region has a higher frequency of occurrence (Figure 8c). The overall frequency of winter drought is relatively high, with only some areas in the southeast having a lower frequency, while the frequency of drought in other areas is above 35% (Figure 8d).

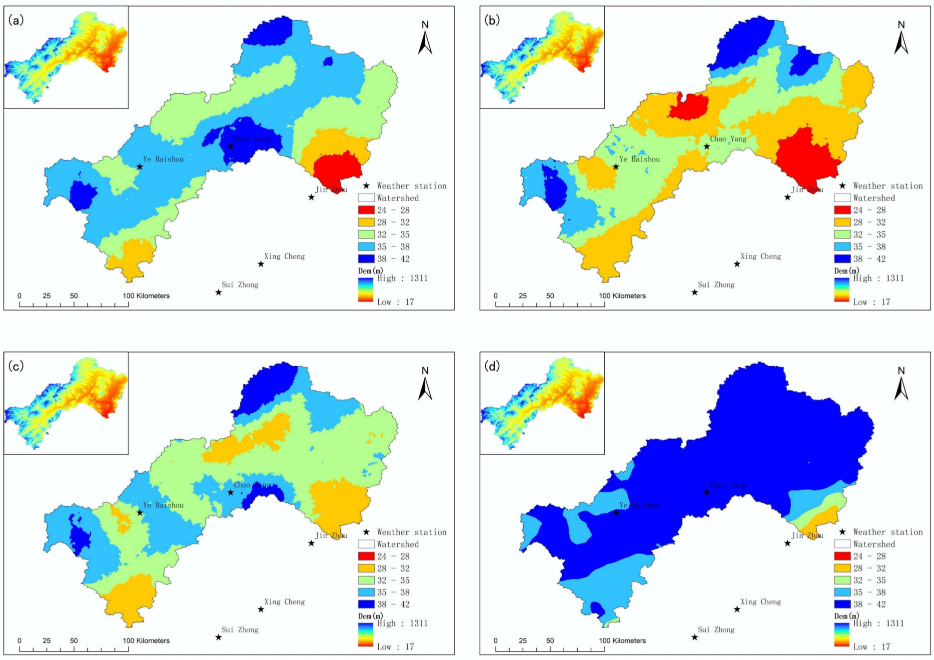

Figure 8. Seasonal drought frequency distribution of Daling River Basin in spring (**a**), summer (**b**), autumn (**c**), and winter (**d**).

4. Distribution characteristics of drought intensity

A continuous drought process was defined as three or more consecutive months experiencing mild drought or worse. The average value of continuous drought processes is used as the drought intensity indicator, with lower values representing more severe droughts. Figure 9 shows that the distribution of drought intensity in Daling River Basin is strongest in the north, followed by the northwest, and weakest in the southeast. This pattern is not entirely consistent with the frequency of drought occurrence, as Chaoyang has a higher frequency of drought occurrence but a weaker drought intensity.

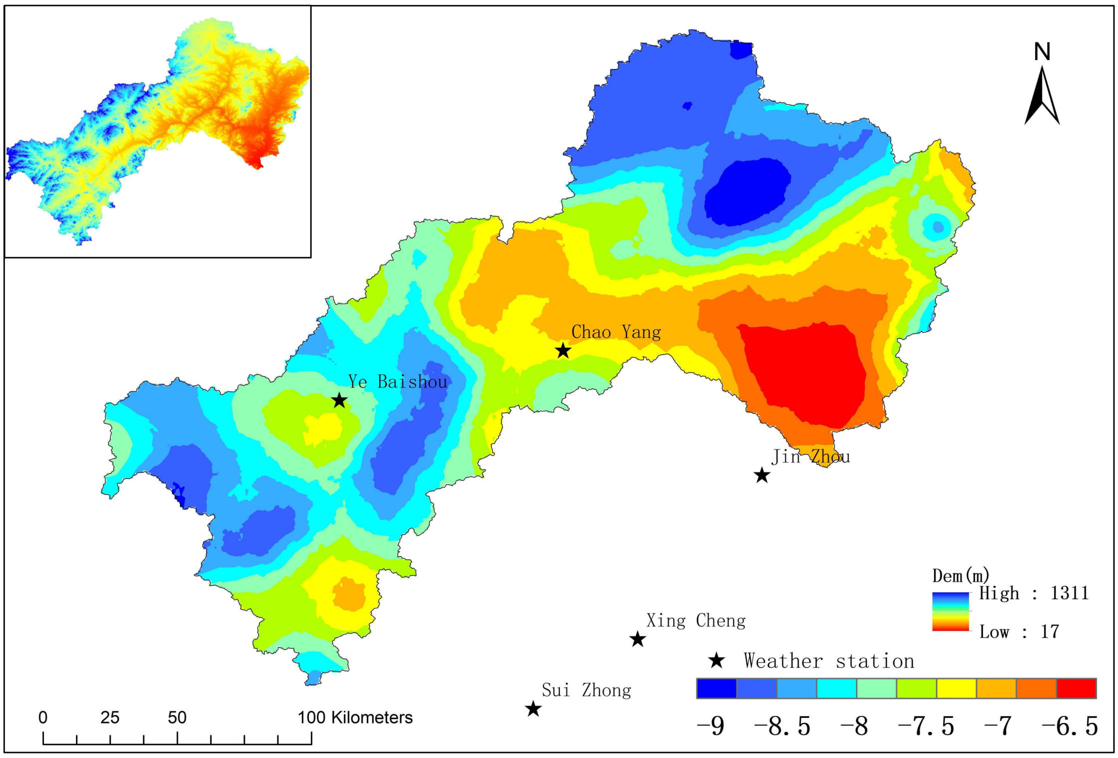

Figure 9. Drought intensity distribution of Daling River Basin.

5. Drought distribution in typical years.

Daling River Basin experienced severe and frequent droughts in 2009–2010, 2011–2012, and 2015–2016. Based on the actual drought losses, it can be inferred that 2009–2010 experienced a relatively severe drought. Therefore, this year was selected as a typical drought year in the Daling River Basin to analyze the spatial distribution characteristics of seasonal changes.

According to Figure 10, from March to June 2009, the entire basin mostly presented slight drought, with a large area of moderate drought beginning in July 2009, and the largest areas of severe and extreme drought occurring in November. According to the spatial distribution of drought in this year, it can also be seen that the severity of drought is proportional to the elevation, and the drought severity presents a trend of spreading from the periphery to the center.

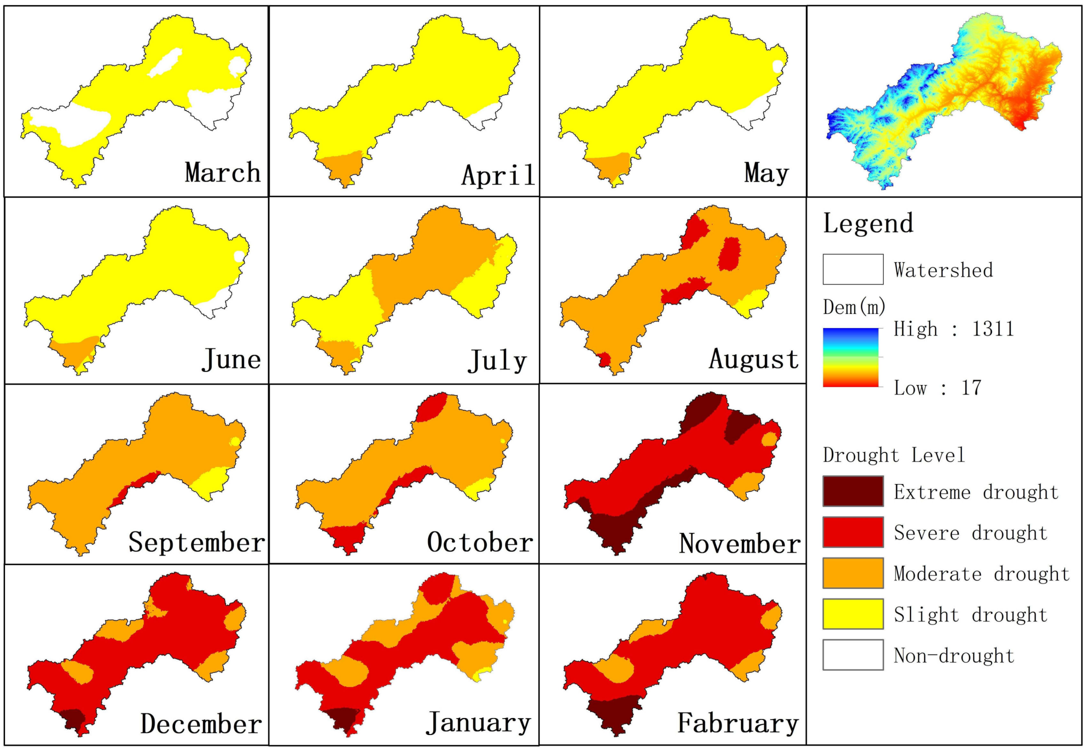

Figure 10. Spatial change in drought from March 2009 to February 2010.

3.3. Analysis of Driving Factors for SMAPI

Reduced precipitation and increased temperature are the main factors causing drought. Changes in global solar radiation can cause changes in atmospheric circulation, leading to drought or flooding in some areas. This study selected precipitation, temperature, and solar radiation as the main meteorological factors affecting drought. The study found that droughts have been exceptionally severe since the beginning of the 21st century, so this study analyzed the factors affecting drought in two periods: 1981–2000 and 2001–2019.

3.3.1. Partial Correlation between *SMAPI* and Major Meteorological Factors

In order to better understand the relationship between *SMAPI* and climate factors, the partial correlation calculation formula (Equation (4)) is used to calculate the partial correlation coefficient between *SMAPI* and precipitation, temperature, and solar radiation, thereby analyzing the correlation between *SMAPI* and major climate factors.

From 1981 to 2000, the partial correlation coefficient between *SMAPI* and precipitation ranged from −0.613 to 0.793 (Figure 11a). A total of 69.52% of the area is positively correlated with precipitation, while 30.48% of the area is negatively correlated. The partial correlation coefficient between *SMAPI* and temperature ranges from −0.408 to 0.292 (Figure 11c). A total of 36.03% of the area is positively correlated with temperature, while 63.97% of the area is negatively correlated. The partial correlation coefficient between *SMAPI* and solar radiation ranges from −0.192 to 0.593 (Figure 11e). A total of 60.05% of the area is positively correlated with solar radiation, while 39.95% is negatively correlated. From 2001 to 2019, the partial correlation coefficient between *SMAPI* and precipitation ranged from −0.778 to 0.509 (Figure 11b). A total of 80.6% of the area is positively correlated with precipitation, while 19.4% of the area is negatively correlated. The partial correlation coefficient between *SMAPI* and temperature ranges from −0.576 to 0.694 (Figure 11d). A total of 17.32% of the area is positively correlated with temperature, while 82.68% is negatively correlated. The partial correlation coefficient between *SMAPI* and solar radiation ranges from −0.337 to 0.55 (Figure 11f). A total of 75.06% of the area is positively correlated with solar radiation, while 24.48% of the area is negatively correlated.

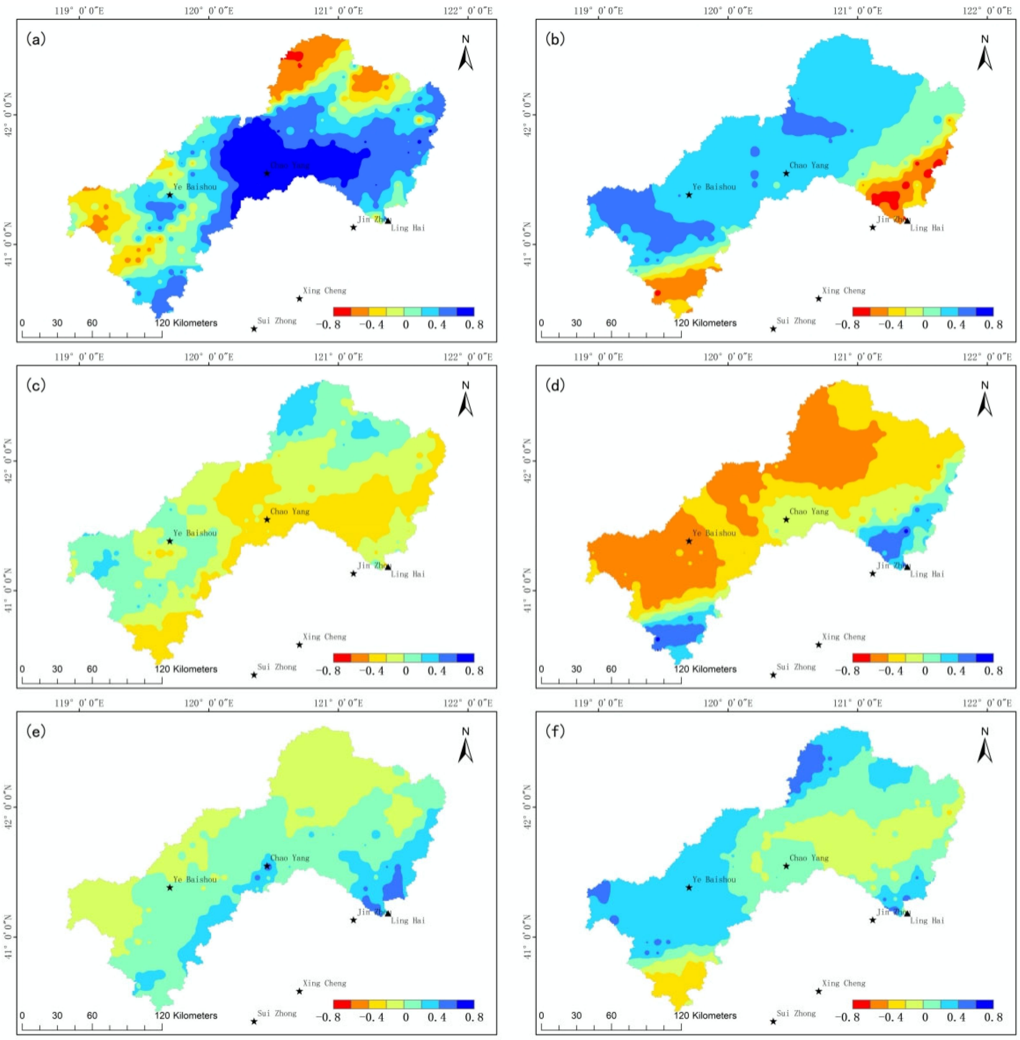

Figure 11. Spatial distributions of partial correlation coefficients between *SMAPI* and precipitation (**a**), temperature (**c**), and solar radiation (**e**) from 1981 to 2000 and the partial correlation coefficients between *SMAPI* and precipitation (**b**), temperature (**d**), and solar radiation (**f**) from 2001 to 2019.

3.3.2. Contribution of Climate Change and Other Factors to *SMAPI*

In order to better understand the contribution of climate change and other factors to *SMAPI*, partial derivative methods were applied to analyze their impact on *SMAPI*. The contributions of climate change and other factors were calculated according to Table 5, as shown in Figure 12 (1981–2000) and Figure 13 (2001–2019). The area of *SMAPI* showed that an upward trend accounted for 61.66%, while the downward trend accounted for 38.34% from 1981 to 2000. In the areas where *SMAPI* had increased, the average contributions of climate change and other factors were 70.14% and 29.86%, respectively (Figure 12a,b). In the areas where *SMAPI* had decreased, the average contributions of climate change and other factors were 37.25% and 62.75%, respectively (Figure 12c,d). Among the areas where *SMAPI* had increased, 79.5% of the area was dominated by climate change, and 20.5% was dominated by other factors. However, in the areas where *SMAPI* had decreased, 66.9% of the area was dominated by other factors and 33.1% was dominated by climate change (Figure 12e,f).

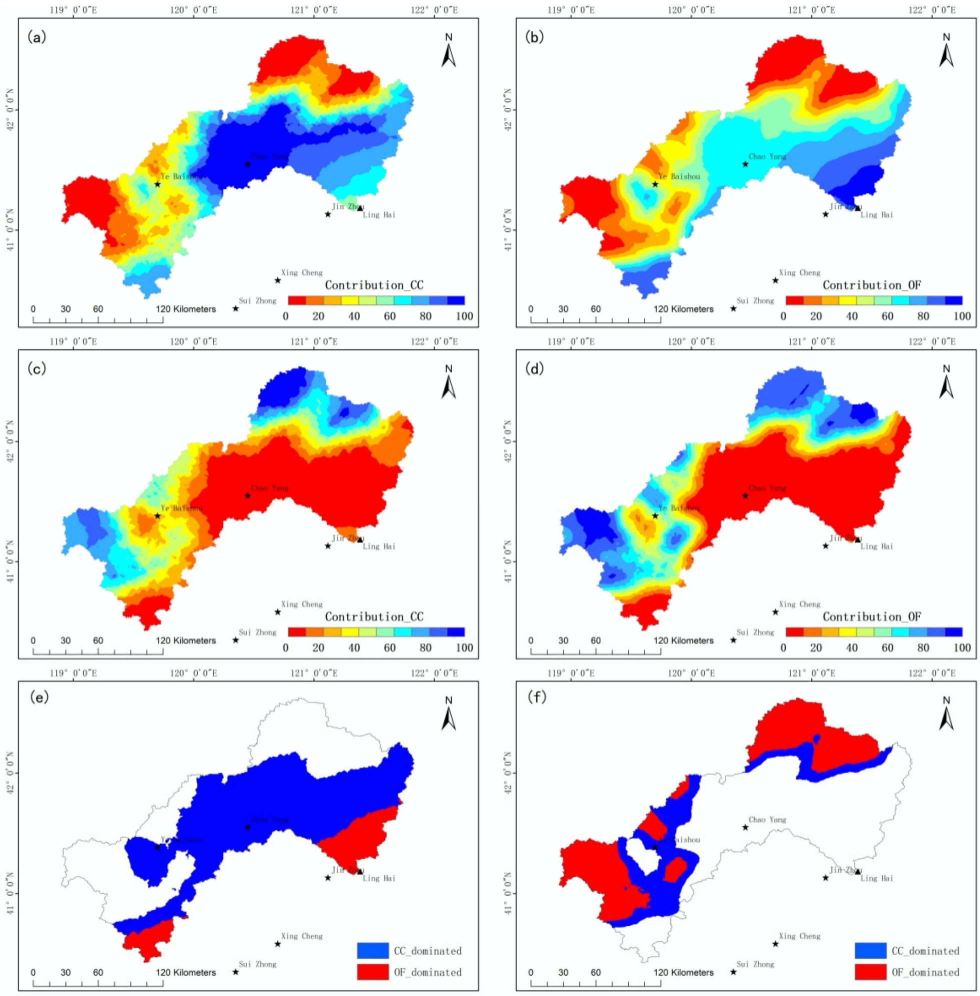

Figure 12. Impacts of climate change and other factors on changes in *SMAPI* from 1981–2010. Contributions to areas with increased (climate change (**a**) and other factors (**b**)) and decreased (climate change (**c**) and other factors (**d**)) *SMAPI*. Spatial distribution of dominant factors on increases (**e**) and decreases (**f**) in *SMAPI*.

Figure 13 shows that *SMAPI* showed an upward trend in 6.47% of the area, with a downward trend accounting for 93.53% from 2001 to 2019. In the areas where *SMAPI* had increased, the average contributions of climate change and other factors were 64.24% and 35.76%, respectively (Figure 13a,b). In the areas where *SMAPI* had decreased, the average contributions of climate change and other factors were 26.25% and 73.75%, respectively (Figure 13c,d). Among the areas where *SMAPI* had increased, 67.9% of the area was dominated by climate change, and 32.1% was dominated by other factors. However, in the areas where *SMAPI* had decreased, 79.8% of the area was dominated by other factors and 20.2% was dominated by climate change (Figure 13e,f).

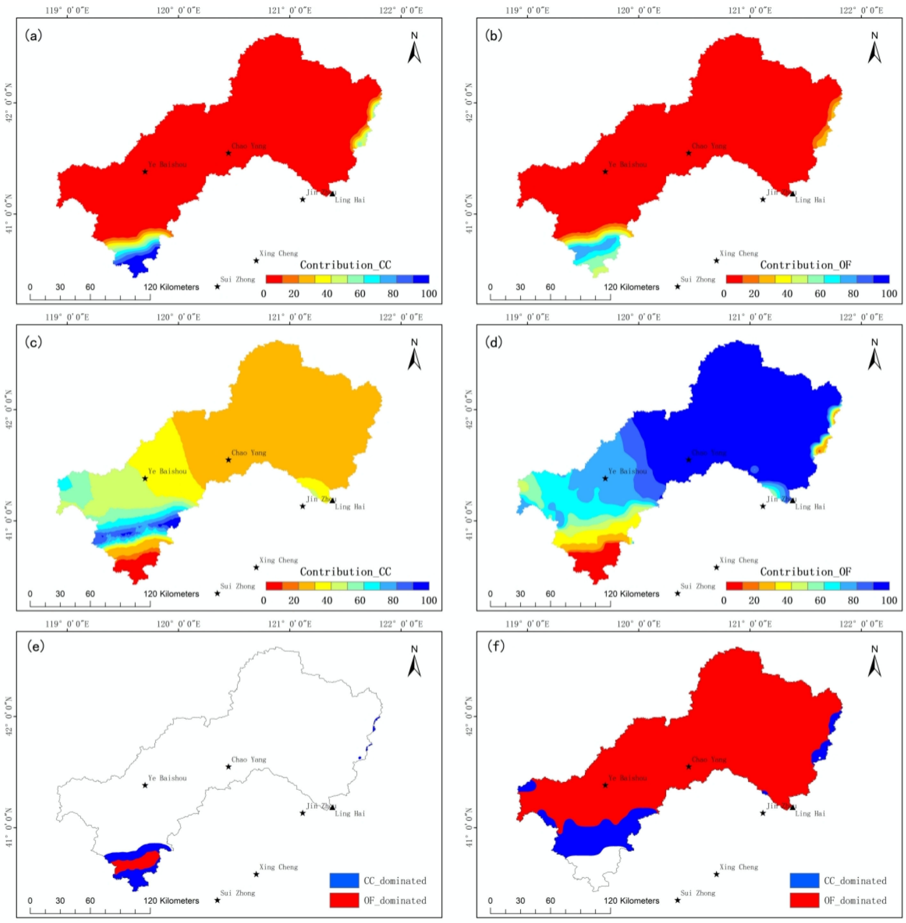

Figure 13. Impacts of climate change and other factors on changes in *SMAPI* from 2001–2019. Contributions to areas with increased (climate change (**a**) and other factors (**b**)) and decreased (climate change (**c**) and other factors (**d**)) *SMAPI*. Spatial distribution of dominant factors on increases (**e**) and decreases (**f**) in *SMAPI*.

4. Discussion

4.1. Drought Characteristics in the Study Area

The Daling River Basin experiences distinct seasonal drought patterns. Wintertime is dominated by dry, cold air flow resulting in little precipitation. Spring is characterized by dry, strong southerly winds leading to high evaporation and limited rainfall. Autumn sees prevailing northerly winds while the summer monsoon brings high temperatures and substantial precipitation. The basin has seen an increasing frequency of severe drought events since 2000, with the 2001–2019 average drought area coverage rate 10 times higher than 1981–2000. Although the distribution of drought frequency and drought intensity in the Daling River Basin is not completely consistent, both tend to be higher in the southeast and southwest compared to the northeast and northwest. The conclusions obtained in this study are basically the same as previous conclusions on the spatio-temporal distribution characteristics of drought. From the 1980s to the 21st century, there was an overall trend of intensification, weakening, and intensification of drought [48]. There are deviations between individual years and seasons, which may be due to previous conclusions mostly considering a meteorological perspective, while this study considers a soil moisture perspective. The high incidence of spring droughts could significantly impact crop growth during the cultivation period, warranting close attention.

4.2. The Impact and Role of CC and OF on SMAPI

Previous studies confirm that climate change significantly impacts agricultural drought, as verified by the strong correlation between *SMAPI* and precipitation, temperature, and solar radiation. Lower *SMAPI* values indicate drier conditions. Precipitation shows a positive correlation with *SMAPI*, as higher rainfall leads to wetter soils. Temperature exhibits a negative correlation, since higher temperatures can increase evapotranspiration and reduce soil moisture, exacerbating drought. Additionally, strong solar radiation melts snow and permafrost, increasing soil moisture. However, excessive radiation may also cause high evaporation rates, worsening drought. Climate change has played a major role in influencing *SMAPI*, while other factors also influence agriculture drought both positively and negatively. The southwest of Daling River Basin is Jianchang County, the southeast is Linghai City, the west is Lingyuan County, and the north is Fuxin Mongol Autonomous County and Naiman County of Inner Mongolia, with a large population distribution. The study found that *SMAPI* mainly showed an upward trend from 1981 to 2000, while *SMAPI* mainly showed a downward trend from 2001 to 2019, which is mainly influenced by other factors. In recent years, urbanization has increased impervious surfaces, reducing infiltration while growing city populations have heightened water consumption. In addition, agricultural production has led to an increase in irrigation water consumption, and the interception and evaporation losses caused by water conservancy projects are also the reasons for drought [49,50]. It is crucial to consider the impacts of climate change and other factors on drought, in order to adopt more targeted drought-resistance measures.

5. Conclusions

Using the VIC model, the research simulated the soil moisture of Daling River Basin and defined the agricultural drought-assessment criteria for the study area based on the *SMAPI*. The spatio-temporal characteristics of agricultural drought were analyzed. The partial derivative methods were applied to evaluate the effects of climate change and other factors on *SMAPI*. The following are the main conclusions drawn from the study:

1. The VIC model adequately simulated the rainfall-runoff process of the Daling River Basin, with Nash efficiency coefficients of 0.58 (calibration) and 0.67 (validation).
2. Drought was most frequent in winter, followed by spring, summer, and autumn. Over 39 years, the basin experienced slight-or-worse drought in 24 years, moderate-or-worse in 15 years, and severe drought in 4 years. Drought frequency from 2001–2019 was 10 times higher compared to 1981–2000.
3. *SMAPI* was positively correlated with precipitation (accounting for 69.52%) and solar radiation (60.05%), while negatively correlated with temperature (63.97%) from 1981 to 2000. From 2001 to 2019, these correlations were 80.6%, 75.06%, and 82.68%, respectively.
4. Climate change was the dominant factor increasing *SMAPI* from 1981–2000, while other factors were the main factors decreasing *SMAPI* from 2001–2019, indicative of intensifying agricultural drought.

This study analyzes the spatio-temporal distribution characteristics and influencing factors of agricultural drought in the Daling River Basin, which has certain reference value for future research on regional agricultural drought. The use of the VIC model, which is based on water balance and energy balance, to simulate soil moisture in the Daling River Basin has improved the limitations of traditional methods and the shortcomings of remote sensing. However, since there are several indicators to evaluate agricultural drought, further research is necessary to explore the use of other drought indicators. Moreover, monitoring and evaluating agricultural drought is essential, and future efforts should focus on predicting drought by using soil moisture as an important indicator.

Author Contributions: Conceptualization, M.D., J.L. and Y.Q.; methodology, M.D. and T.J.; data curation, M.D. and Y.Q.; writing—original draft, M.D.; writing—review and editing, Y.Q. and T.J.; supervision, J.L. All authors have read and agreed to the published version of the manuscript.

Funding: This research was funded by the National Key Research and Development Program Funded Project, grant number 2023YFC3006604, The Ministry of Water Resources' Flood and Drought Disaster Prevention Strategy Research Talent Innovation Team Project, grant number WH0145B042021 and the

Special Project of Basic Scientific Research Business Expenses of China Academy of Water Resources and Hydropower Research, grant number JZ110145B0032023.

Data Availability Statement: The data used during the study appear in the submitted article.

Conflicts of Interest: The authors declare no conflict of interest. The funders had no role in the design of the study, in the collection, analyses, or interpretation of data, in the writing of the manuscript, or in the decision to publish the results.

References

1. He, L.; Qin, Q.; Ren, H.; Du, J.; Meng, J.; Du, C. Retrieving farmland surface soil moisture using multi temporal Sentinel-1 SAR data. *J. Agric. Eng.* **2016**, *32*, 142–148.
2. Legates, R.D. Soil moisture: A central and unifying theme in physical geography. *Prog. Phys. Geogr.* **2011**, *35*, 65–86. [CrossRef]
3. Cai, S.; Song, X.; Hu, R.; Leng, P.; Li, X.; Guo, D.; Hao, Y.; Wang, Y. Spatiotemporal characteristics of agricultural droughts based on soil moisture data in Inner Mongolia from 1981 to 2019. *J. Hydrol.* **2021**, *603*, 127104. [CrossRef]
4. Possega, M.; Ojeda, V.G.M.; Fortis, G.R.S. Multi-Scale Analysis of Agricultural Drought Propagation on the Iberian Peninsula Using Non-Parametric Indices. *Water* **2023**, *15*, 2032. [CrossRef]
5. Baik, J.; Zohaib, M.; Kim, U.; Aadil, M.; Choi, M. Agricultural drought assessment based on multiple soil moisture products. *J. Arid. Environ.* **2019**, *167*, 43–55. [CrossRef]
6. Ajaz, A.; Taghvaeian, S.; Khand, K.; Gowda, P.H.; Moorhead, J.E. Development and Evaluation of an Agricultural Drought Index by Harnessing Soil Moisture and Weather Data. *Water* **2019**, *11*, 1375. [CrossRef]
7. Chen, S.; Liu, Y.; Wen, Z. Review on the study of retrieving soil moisture by satellite remote sensing. *Prog. Earth Sci.* **2012**, *27*, 1192–1203.
8. Li, B.; Zhou, G. Advance in the study on drought index. *Acta Ecol. Sin.* **2014**, *34*, 1043–1052.
9. Wu, Z.; Lu, G.; Guo, H.; Kuang, Y. Drought monitoring technology based on simulated soil moisture. *J. Hohai Univ. Nat. Sci. Ed.* **2012**, *40*, 28–32.
10. Lu, G.; Kuang, Y.; Wu, Z.; He, H. Analysis of spatio-temporal characteristics of simulated soil moisture in different climatic regions of China. *China's Rural. Water Conserv. Hydropower* **2013**, *5*, 15–19.
11. Wu, Z.; Xu, Z.; Xiao, H.; Wu, H. Analysis of the spatio-temporal characteristics of drought events in the upper reaches of the Yangtze River based on simulated soil moisture. *Resour. Environ. Yangtze River Basin* **2018**, *27*, 176–184.
12. Zhang, J.; Zhang, Q.; Zhao, H.; Zhang, P. Principle and application of quantitative remote sensing inversion of crop water potential. *J. Ecol.* **2008**, *27*, 916–923.
13. Liang, X.; Lettenmaier, D.P.; Wood, E.F.; Burges, S.J. A simple hydrologically based model of land surface water and energy fluxes for general circulation models. *J. Geophys. Res. Atmos.* **1994**, *99*, 14415–14428. [CrossRef]
14. Liang, X.; Wood, E.F.; Lettenmaier, D.P. Surface soil moisture parameterization of the VIC-2L model: Evaluation and modification. *Glob. Planet. Chang.* **1996**, *13*, 195–206. [CrossRef]
15. Wang, H.; Rogers, J.C.; Munroe, D.K. Commonly Used Drought Indices as Indicators of Soil Moisture in China. *J. Hydrometeorol.* **2015**, *16*, 1397–1408. [CrossRef]
16. Zhu, Y.; Liu, Y.; Ma, X.; Ren, L.; Singh, V.P. Drought Analysis in the Yellow River Basin Based on a Short-Scalar Palmer Drought Severity Index. *Water* **2018**, *10*, 1526. [CrossRef]
17. Fan, Y.; Dool, H.V.D. Climate Prediction Center global monthly soil moisture data set at 0.5° resolution for 1948 to present. *J. Geophys. Res. Atmos.* **2004**, *109*, D10102. [CrossRef]
18. Leng, G.; Tang, Q.; Rayburg, S. Climate change impacts on meteorological, agricultural and hydrological droughts in China. *Glob. Planet. Chang.* **2015**, *126*, 23–34. [CrossRef]
19. Wu, Z.Y.; Lu, G.H.; Wen, L.; Lin, C.A. Reconstructing and analyzing China's fifty-nine year (1951–2009) drought history using hydrological model simulation. *Hydrol. Earth Syst. Sci.* **2011**, *8*, 2881–2894. [CrossRef]
20. Taká, J. Assessment of Drought in Agricultural Regions of Slovakia Using Soil Water Dynamics Simulation. *Agriculture* **2013**, *59*, 74–87. [CrossRef]
21. Wang, C.; Guo, J.; Chen, H.; Liu, X. Drought dynamic monitoring indicators based on soil moisture simulation and their applicability. *J. Ecol.* **2011**, *30*, 7.
22. Du, C.; Chen, J.; Nie, T.; Dai, C. Spatial–temporal changes in meteorological and agricultural droughts in Northeast China: Change patterns, response relationships and causes. *Nat. Hazards* **2021**, *110*, 155–173. [CrossRef]
23. Qin, D. *National Assessment Report on Extreme Weather Climate Events and Disaster Risk Management and Adaptation in China*; Science Press: Beijing, China, 2015; pp. 70–71.
24. Yin, X.; Yang, L.; Wang, X. Hydrological characteristics analysis of Daling River basin. *Agric. Technol.* **2007**, *27*, 168–171.
25. Liu, X. Study on flood and drought law and runoff simulation in Linghe River basin. Dissertation, Shenyang Agricultural University, Shenyang, China, 2015.
26. Liang, X.; Xie, Z. A new surface runoff parameterization with subgrid-scale soil heterogeneity for land surface models. *Adv. Water Resour.* **2001**, *24*, 1173–1193. [CrossRef]

27. Liang, X.; Xie, Z. Important factors in land–atmosphere interactions: Surface runoff generations and interactions between surface and groundwater. *Glob. Planet. Chang.* **2003**, *38*, 101–114. [CrossRef]
28. Zhao, Q.; Ye, B.; Ding, Y.; Zhang, S.; Yi, S.; Wang, J.; Shangguan, D.; Zhao, C.; Han, H. Coupling a glacier melt model to the Variable Infiltration Capacity (VIC) model for hydrological modeling in north-western China. *Environ. Geol.* **2013**, *68*, 87–101. [CrossRef]
29. Zhao, R. *Hydrologic Simulation of Basin: Xin'anjiang Model and Northern Shaanxi Model*; Water Resources and Electric Power Press: Nanjing, China, 1984.
30. Nijssen, B.; Schnur, R.; Lettenmaier, D.P. Global Retrospective Estimation of Soil Moisture Using the Variable Infiltration Capacity Land Surface Model, 1980–1993. *J. Clim.* **1999**, *14*, 1790–1808. [CrossRef]
31. Hamlet, A.F.; Mote, P.W.; Clark, M.P.; Lettenmaier, D.P. Twentieth-Century Trends in Runoff, Evapotranspiration, and Soil Moisture in the Western United States. *J. Clim.* **2007**, *20*, 1468–1486. [CrossRef]
32. Zhang, Y.; Wu, Z.; He, H. Agricultural drought assessment based on hydrological crop coupling model and CWAPI index. *J. Water Resour.* **2022**, *53*, 1168–1179.
33. Zhang, B.; Wu, P.; Zhao, X.; Wang, Y.; Gao, X.; Cao, X. A drought hazard assessment index based on the VIC–PDSI model and its application on the Loess Plateau, China. *Theor. Appl. Climatol.* **2013**, *114*, 125–138. [CrossRef]
34. Zhang, Y.; You, Q.; Chen, C.; Li, X. Flash droughts in a typical humid and subtropical basin: A case study in the Gan River Basin, China. *J. Hydrol.* **2017**, *551*, 162–176. [CrossRef]
35. Wu, Z.; Lu, G.; Wen, L.; Lin, C.A.; Zhang, J.; Yang, Y. Thirty-Five Year (1971–2005) Simulation of Daily Soil Moisture Using the Variable Infiltration Capacity Model over China. *Atmosphere-Ocean* **2007**, *45*, 37–45. [CrossRef]
36. Zhang, Y.; Deng, L.; Yan, W.; Shangguan, Z.P. Interaction of soil water storage dynamics and long-term natural vegetation succession on the Loess Plateau, China. *Catena* **2016**, *137*, 52–60. [CrossRef]
37. Ge, W.; Deng, L.; Wang, F.; Han, J. Quantifying the contributions of human activities and climate change to vegetation net primary productivity dynamics in China from 2001 to 2016. *Sci. Total Environ.* **2021**, *773*, 145648. [CrossRef] [PubMed]
38. Peng, Q.; Wang, R.; Jiang, Y.; Li, C. Contributions of climate change and human activities to vegetation dynamics in Qilian Mountain National Park, northwest China. *Glob. Ecol. Conserv.* **2021**, *32*, e01947. [CrossRef]
39. Burrell, L.A.; Evans, P.J.; Liu, Y. Detecting dryland degradation using Time Series Segmentation and Residual Trend analysis (TSS-RESTREND). *Remote Sens. Environ.* **2017**, *197*, 4. [CrossRef]
40. Luo, L.; Ma, W.; Zhuang, Y.; Zhang, Y.; Yi, S.; Xu, J.; Long, Y.; Ma, D.; Zhang, Z. The impacts of climate change and human activities on alpine vegetation and permafrost in the Qinghai-Tibet Engineering Corridor. *Ecol. Indic.* **2018**, *93*, 24–35. [CrossRef]
41. Xie, Z.; Yuan, F. A parameter estimation scheme of the land surface model VIC using the MOPEX databases. *IAHS Publ.* **2006**, *307*, 169.
42. Huang, M.; Xu, L. On the assessment of the impact of reducing parameters and identification of parameter uncertainties for a hydrologic model with applications to ungauged basins. *J. Hydrol.* **2006**, *320*, 37–61. [CrossRef]
43. Nash, J.E.; Sutcliffe, J.V. River flow forecasting through conceptual models part I â A discussion of principles. *J. Hydrol.* **1970**, *10*, 282–290. [CrossRef]
44. Sun, S.; Wang, Y. Analysis of Summer Drought in Liaoning Province in 2006. *Northeast Water Resour. Hydropower* **2007**, *276*, 31–33.
45. Shi, Z. Study on Comprehensive Drought Index of Daling River Basin Based on Hydrological model. *Water Resour. Plan. Des.* **2016**, *4*, 48–51.
46. Sun, C.; Wang, L.; Wu, J. Analysis of the current situation of water resources in the Daling River basin and countermeasures for sustainable utilization. *South North Water Divers. Water Conserv. Sci. Technol.* **2007**, *2*, 46–49.
47. Liu, Q.; Gao, L.; Ma, M.; Wang, L.; Lin, H. Study on the downscaling of temperature and precipitation in Daling River Basin, Liaoning. *Water Resour. Hydropower Technol.* **2021**, *52*, 16–31, (In Chinese and English).
48. Zhang, Y.; Fang, Y. Gong Qiang Spatial and temporal characteristics of drought during the growing season in Liaoning Province based on SPEI index. *J. Ecol.* **2017**, *36*, 8.
49. Zhang, D.; Zhou, H. Study on the change trend and causes of water resources in the upper reaches of Daling River Basin. *Hydrology* **2011**, *31*, 81–87. [CrossRef]
50. Wu, L.; Zhang, A. Impact of climate change and human activities on runoff in the upper reaches of Daling River. *Prog. Water Resour. Hydropower Sci. Technol.* **2016**, *36*, 10–15.